All-Dielectric Transformed Material for Microwave Broadband Orbital Angular Momentum Vortex Beam

Jianjia Yi,[1,*] Xueqi Cao,[1] Rui Feng,[1,2] Badreddine Ratni,[3] Zhihao Jiang,[4] Danny Zhu,[5] Lina Zhu,[1,†] André de Lustrac,[2] Douglas H. Werner,[6] and Shah Nawaz Burokur[3,‡]

[1] *Key Laboratory of Integrated Services Networks, Xidian University, No. 2 South Taibai Road, Xi'an, 710071 Shaanxi, China*

[2] *Centre de Nanosciences et de Nanotechnologies, CNRS, Université Paris-Saclay, 10 Boulevard Thomas Gobert, 91120 Palaiseau, France*

[3] *LEME, Université Paris Nanterre, 92410 Ville d'Avray, France*

[4] *State Key Laboratory of Millimeter Waves, Southeast University, Nanjing, 210096 Jiangsu, China*

[5] *Department of Electrical Engineering and Computer Science, U.S. Military Academy, West Point, New York 10996, USA*

[6] *Department of Electrical Engineering, The Pennsylvania State University, University Park, Pennsylvania 16802, USA*

(Received 13 July 2019; revised manuscript received 12 August 2019; published 30 August 2019)

Electromagnetic waves exhibiting vortex properties from orbital angular momentum (OAM) modes that are inherently orthogonal show promising potential for a wide range of applications. However, classic OAM-wave generators in the radio-frequency band are generally limited by a narrow operation bandwidth, complicated feeding structures, or high losses. In this work, we propose a method for OAM-wave generation using the concept of spatial transformation at microwave frequencies. A reflection-type vortex-beam generator is designed and simulated. Then an all-dielectric proof-of-concept prototype for a +1 topological charge is physically implemented and the complete characterization of the device is reported. Both full-wave simulations and experimental measurements successfully validate the spiral-shaped phase fronts of the vortex wave. Furthermore, the all-dielectric implementation of the device enables operation over a broad frequency bandwidth. The proposed method provides an efficient approach to generate vortex waves carrying OAM modes and illustrates the practicality of using spatial transformations to achieve an alternative class of optical devices at microwave frequencies.

DOI: 10.1103/PhysRevApplied.12.024064

I. INTRODUCTION

Angular momentum of electromagnetic waves can be divided into two classes; namely, spin angular momentum and orbital angular momentum (OAM) [1]. Spin angular momentum is related only to the spin of a photon and is characterized by a circular polarization state. Orbital angular momentum depends on the field spatial distribution and is associated with the beam vorticity and phase singularity, which imparts to the electromagnetic wave a helical transverse phase distribution. Therefore, an electromagnetic wave carrying OAM modes is referred to as a vortex electromagnetic wave that presents a phase quantified by $e^{il\varphi}$ in its wave front, where l is the intrinsic value of orbital angular momentum ($l = 0, \pm 1, \pm 2$) and φ is the transverse azimuthal angle [2]. OAM vortex waves with different topological modes are mutually orthogonal to each other, an important property that has inspired a large number of researchers to explore their intriguing physical properties throughout the whole electromagnetic spectrum. OAM vortex waves in the microwave regime can find potential applications in the fields of data transmission, radar imaging, target detection, and sensing [3–7].

Because of the fascinating properties and numerous potential applications of OAM waves, different methods have been proposed to generate OAM beams in the radio-frequency (rf) band, including antenna arrays [8,9], metasurfaces [10–13], spiral phase plates [14,15], and helicoidal parabolic antennas [16]. Among these methods, antenna arrays have been extensively studied in the past several years. However, the main drawback is that a complicated feeding network is required to generate a radiated wave with a spiral phase profile. When the desired topological charge of orbital angular momentum is large, a high number of radiating elements are required, which significantly increases the design and feeding complexities of the

*jianjia.yi@xidian.edu.cn
†lnzhu@xidian.edu.cn
‡sburokur@parisnanterre.fr

system. On the other hand, using a metasurface to generate OAM waves possesses several advantages, such as high gain, a small divergence angle, a low-profile structure, and an easy fabrication process. However, this approach generally suffers from a narrow bandwidth or low efficiency. The spiral phase plate is the most widely used, and is characterized by a straightforward theory and simple structure, while offering high conversion efficiency. Nevertheless, in the rf band, the divergence angle of the generated beam is not convenient for long-distance transmission and the structure responds only to a specific frequency. Finally, the helicoidal parabolic antenna is also an effective device with high efficiency. It is essentially composed of a reflecting rotating phase plate designed as a parabolic dish with a single radial cut introduced on the surface. A spherical wave front emitted by a feed antenna located at the parabola's focal point is reflected, forming a directive outgoing vortex beam. However, because of the irregular shape and bulkiness of the helicoidal parabolic antenna, its integration in practical communication systems is not very straightforward. Compared with the optical regime, the generation of vortex beams in the rf band depends mostly either on complex structures that are difficult to integrate or on the feeding and coupling circuits, which lead to narrow bandwidth. To address these shortcomings, it is necessary to pursue a technology that can achieve OAM-wave generation while simultaneously offering a compact form factor, planar device configuration, and broad operational bandwidth.

Spatial transformation is a well-known approach to control electromagnetic fields in unprecedented ways through the use of judiciously engineered materials with spatially varying parameters. Although the theoretical basis first appeared a few decades ago, the correspondence between the transformed medium and material parameters was not formally established until 2006 [17,18]. Neumann and Dirichlet sliding boundary conditions are set at the limits of the transformation zones to establish a quasiconformal mapping between the physical and virtual domains. The transformed material parameters are determined by the solution of Laplace's equation. This concept offers a technique that is capable of manipulating incident electromagnetic fields to tailor complex and desired spatial patterns, providing a diverse range of applications in engineering and applied sciences, such as invisibility cloaking [19,20], focusing devices [21–24], multibeam lens antennas [25,26], and other wave-front-manipulated devices.

In this paper, according to the concept of spatial transformation, we present an all-dielectric microwave device that is capable of generating OAM electromagnetic waves with mode +1 in the reflection state. By solving Laplace's equation under proper Dirichlet and Neumann boundary conditions, we establish the transformation mapping between the virtual-space and physical space zones. Thus, for a practical implementation of the device, eight constituent sectors representing different phase variations are extracted from the calculations to cover the total phase range of 2π necessary for vortex-beam generation. Each sector has similar physical dimensions but a different effective-permittivity distribution. The design for the proposed all-dielectric device is presented along with numerical simulations predicting its performance. Furthermore, a reflection-mode prototype capable of generating an electromagnetic wave carrying an OAM mode $l = +1$ in the microwave domain is fully implemented by dielectric three-dimensional (3D) printing, and exhibits qualitatively good agreement between simulated and measured results. Importantly, because of the use of nonresonant metamaterial structures, the device possesses a substantial broad operational bandwidth.

II. DESIGN OF THE OAM-VORTEX-BEAM-GENERATION DEVICE

The spatial-transformation-based generation method is schematically presented in Fig. 1. A helicoidal parabolic structure composed of several discrete surfaces is considered. One of the surfaces having a central angle of $\varphi = \pi/4$ is shown in Fig. 1(a) for illustrative purposes. When an electromagnetic beam is incident on the surface, the different regions of the wave front produce relative phase delays due to the nonplanar spiral structure of the metal parabola, thus achieving the effect of wave-front twisting. Based on the concept of spatial transformation, a flat device that performs the same function as the helicoidal parabolic reflector is shown in Fig. 1(b).

The curved surface DEF and planar surface $D'E'F'$ are perfect-electric-conductor boundaries. The thickness of the physical spaces in the reflective device is set as a constant L. Neumann and Dirichlet sliding boundary conditions are set at the edges of the device as follows:

$$\begin{aligned} &r'|_{AB,BC,AC,TD,AD,CF,BE} = r, \\ &\mathbf{n}\cdot\nabla r'|_{EF,DE} = 0, \end{aligned} \tag{1}$$

$$\begin{aligned} &z'|_{AB,BC,AC} = 0, \\ &z'|_{EF,DE} = \tfrac{M}{N^2}r^2 - (K+M), \\ &\mathbf{n}\cdot\nabla z'|_{BE,AD,CF,DF} = 0, \end{aligned} \tag{2}$$

where $\mathbf{n}$ is the vector normal to the boundaries of the surface. The detailed design of the OAM-vortex-beam-generation device is presented in Supplemental Material [27].

To obtain the expected mapping between free space and the physical space, the partial-differential-equation solver COMSOL MULTIPHYSICS is used to solve Laplace's equation subject to the defined boundary conditions. In our design, the geometry parameters denoted in Fig. 1 are as follows: $N = 105$ mm, $L = 35$ mm, and $M = 19.23$ mm. The physical

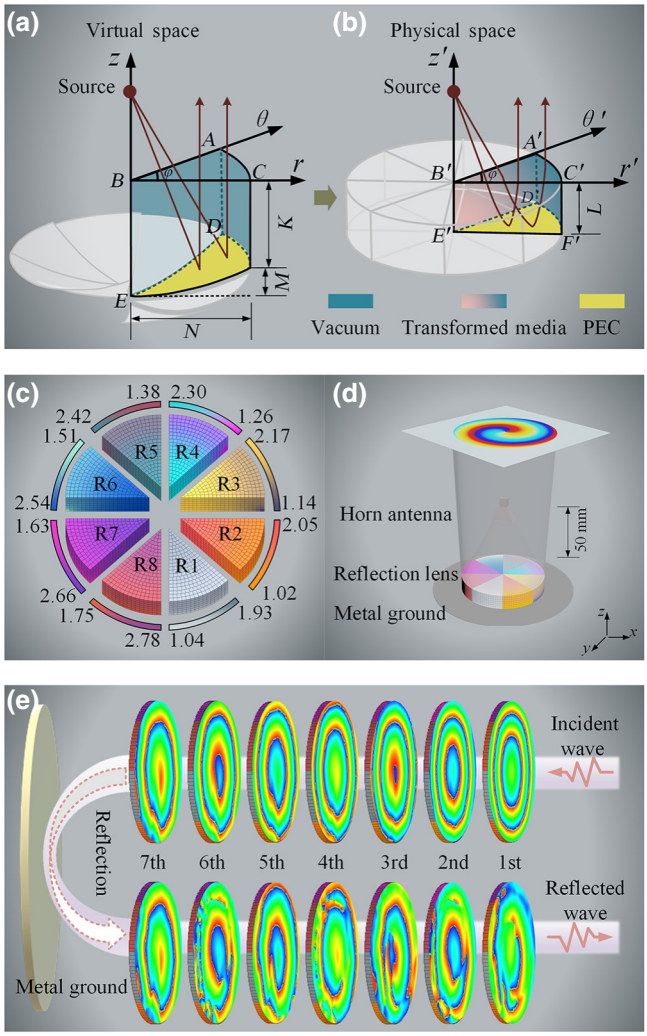

FIG. 1. Spatial transformation from virtual space to physical space, where the curved virtual space is transformed into the proposed OAM-generation-device design: (a) virtual space and (b) physical space of the reflection-type device. (c) Calculated permittivity distributions of the OAM generator. (d) Operating principle of the device. (e) Phase variation of the incident wave after passing through each layer of the vortex-beam generator at 12 GHz. PEC, perfect electric conductor.

dimension of each elementary unit is set to $5 \times 5 \times 5\ \mathrm{mm}^3$. Moreover, each proposed sector is discretized into seven layers along the z' axis and each layer consists of 21 circular rings. As a result, the entire device with an oblate cylindrical shape is composed of 1176 different circular rings containing a total of 9576 cubical unit cells. Through simulation and optimization of the variable K, eight sectors for the device with different permittivity distributions are used, as presented in Fig. 1(c). According to the continuous permittivity distribution, the entire space is discretized into a plurality of building blocks with similar size. The permittivity of each sector shares a similar distribution but different range, while the phase variation between adjacent sectors is $\pi/4$. It is worthwhile noting that with ordered combinations of such sectors, the transformed medium can be engineered in an effective manner to generate vortex beams carrying OAM.

III. RESULTS AND DISCUSSION

Full-wave simulations are performed to verify the functionalities of the OAM-beam-generation device with the finite-element-method-based program HFSS at 12 GHz. A regular X-band horn antenna emitting quasispherical waves located along the central axis of the microwave device is used as the feeding source and is placed 50 mm ($2\lambda_0$ at 12 GHz, with λ_0 being the free-space wavelength) from the upper surface of the device. The functionality of the reflection-type generator is numerically characterized as illustrated in Fig. 1(d), where the designed transformation medium is backed by a circular reflecting metal plate.

Since the corresponding refractive index and wavelength of the electromagnetic wave are different in different media, the ray path and propagation period of the incident wave will change when the electromagnetic wave propagates in the device. To further observe the phase change of the incident wave inside the transformed medium, the phase profiles are simulated in each layer at 12 GHz and are plotted in Fig. 1(e). It can be clearly observed how the quasispherical wave is transformed to the vortex wave inside the device step-by-step after being reflected on the metal plate.

The phase distributions and intensity patterns of the electric field in a plane normal to the direction of propagation as well as characteristics of the far-field patterns in the **E** plane (x-o-z plane containing **E** and **k** vectors) and **H** plane (y-o-z plane containing **H** and **k** vectors) obtained from numerical simulations are depicted in Fig. 2. The helical phase distribution [Fig. 2(a)], characteristic of an electromagnetic wave carrying an OAM mode, is clearly revealed in the simulated data, which indicate that vortex beams with a topological charge $l = +1$ are indeed generated by the permittivity distributions used in the device. The simulated intensity profiles are illustrated in Fig. 2(b), where an amplitude null in the center of the beam can be clearly seen, which is the main feature of electromagnetic waves carrying OAM. The two-dimensional far-field radiation patterns show beams with a hollow main lobe [Fig. 2(c)], which is also an intrinsic characteristic of vortex beams, provide further evidence that the generated beam carries an OAM mode.

Moreover, the phase and intensity profiles of the near-field distributions for mode $l = +1$ are further compared from 8 to 16 GHz, demonstrating that the OAM-generation device is capable of retaining performance over a broad frequency range. Theoretically, the achieved bandwidth can be very broad since all-dielectric nonresonant

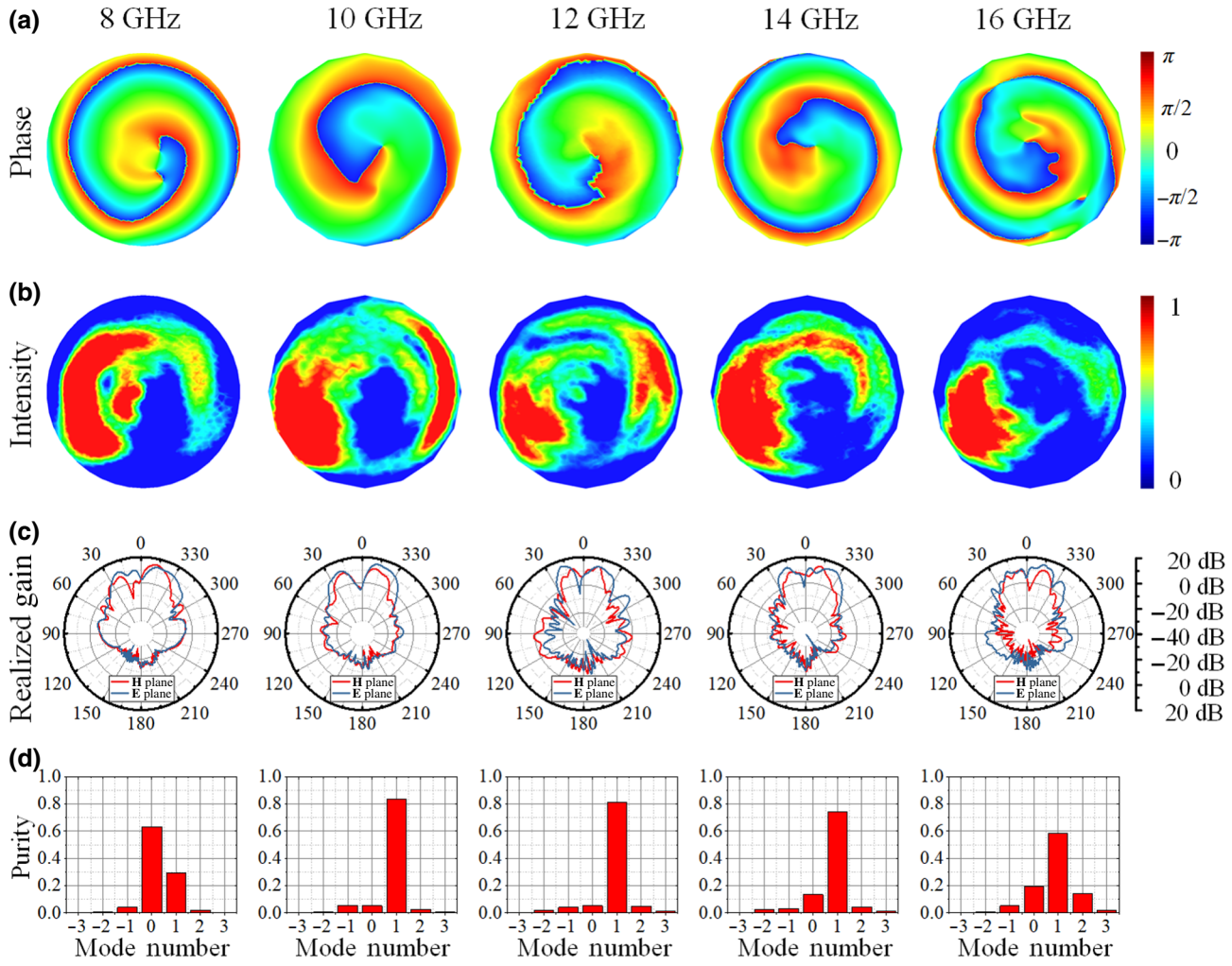

FIG. 2. Numerical simulation results for the OAM-generation device with mode $l = +1$ in a frequency range from 8 to 16 GHz. (a) Phase diagrams of the electric field. The resulting phase varies from $-180°$ (blue) to $180°$ (red). (b) Intensity distributions of the electromagnetic field in the x-o-y plane. (c) Two-dimensional far-field radiation patterns in the **E** and **H** planes of the device, where a characteristic "bunny-ear"-shaped diagram is obtained. (d) Calculated mode spectra of the generated $l = +1$ OAM beam.

materials are used in the design. However, for realistic discrete structures, the design dimensions and unit-cell periodicity limit the operating bandwidth.

The corresponding power distributions of the proposed device are analyzed on the basis of the purity calculation of OAM modes. Since the azimuthal angle φ is a periodic function, its Fourier conjugate, which is the OAM wave, is a discrete variable. The linking Fourier relationship is given by [28]

$$A_l = \frac{1}{2\pi}\int_0^{2\pi} \psi(\varphi) d\varphi e^{-jl\varphi}, \tag{3}$$

$$\psi(\varphi) = \sum_l A_l e^{jl\varphi}. \tag{4}$$

The calculated results at different frequencies are shown in Fig. 2(d). At a frequency of 8 GHz, the total phase deflection after the phase plate does not reach 2π, and therefore in the expansion of the Fourier transform, part of the generated OAM waves is decomposed into modes $l = 0$ and $l = +1$. We can observe that the expected OAM mode $l = +1$ is relatively dominant at 10, 12, 14, and 16 GHz, which indicates the high quality of the generated OAM beams. To experimentally validate the proposed spatial-transformation approach, a prototype of the reflection-type device generating a vortex beam carrying the OAM mode $l = +1$ is physically realized. To achieve this, first a 3D model of the all-dielectric device is designed for implementation. To realize permittivities ranging from 1 to 2.8, two kinds of meta-atom structures are adopted, as illustrated in Fig. 3(a). The elementary meta-atom is composed of three orthogonally crossed cylinders in a cubic region of $5 \times 5 \times 5$ mm^3 ($\lambda_0/5$ at 12 GHz). The effective relative permittivity of a unit cell depends on the radius

of the cylinders. To ensure a smooth connection between adjacent cells, the meta-atom can be bent and trimmed appropriately. The prototype of the designed device is then fabricated by a Stratasys Objet260 Connex3 polymer jetting 3D printer [29] with use of a VeroWhite dielectric material, which has relative permittivity $\varepsilon_h = 2.8$ in the frequency band of interest. A photograph of the printed flat cylindrical device, which consists of 9576 unit cells, with a height of 35 mm and a base radius of 105 mm, is presented in Fig. 3(b).

Two experimental setups are used to validate the functionality of the OAM-generation device. First, the electric field is scanned with a field-sensing fiber-optic active antenna probe capable of measuring both the intensity and the phase of the electric field through a vector network analyzer. Hence, at the receiving end, the probe, which is connected to the network analyzer via a coaxial cable, is mounted on two orthogonal computer-controlled linear-motion stages. A quasispherical wave is emitted along the z direction by a regular X-band horn antenna placed 50 mm directly in front of the device. The measurement setup is illustrated in Fig. 3(c). The all-dielectric device, metal plate, and probe are placed in the x-o-y plane. By stepping the field-sensing probe in increments of 2 mm and

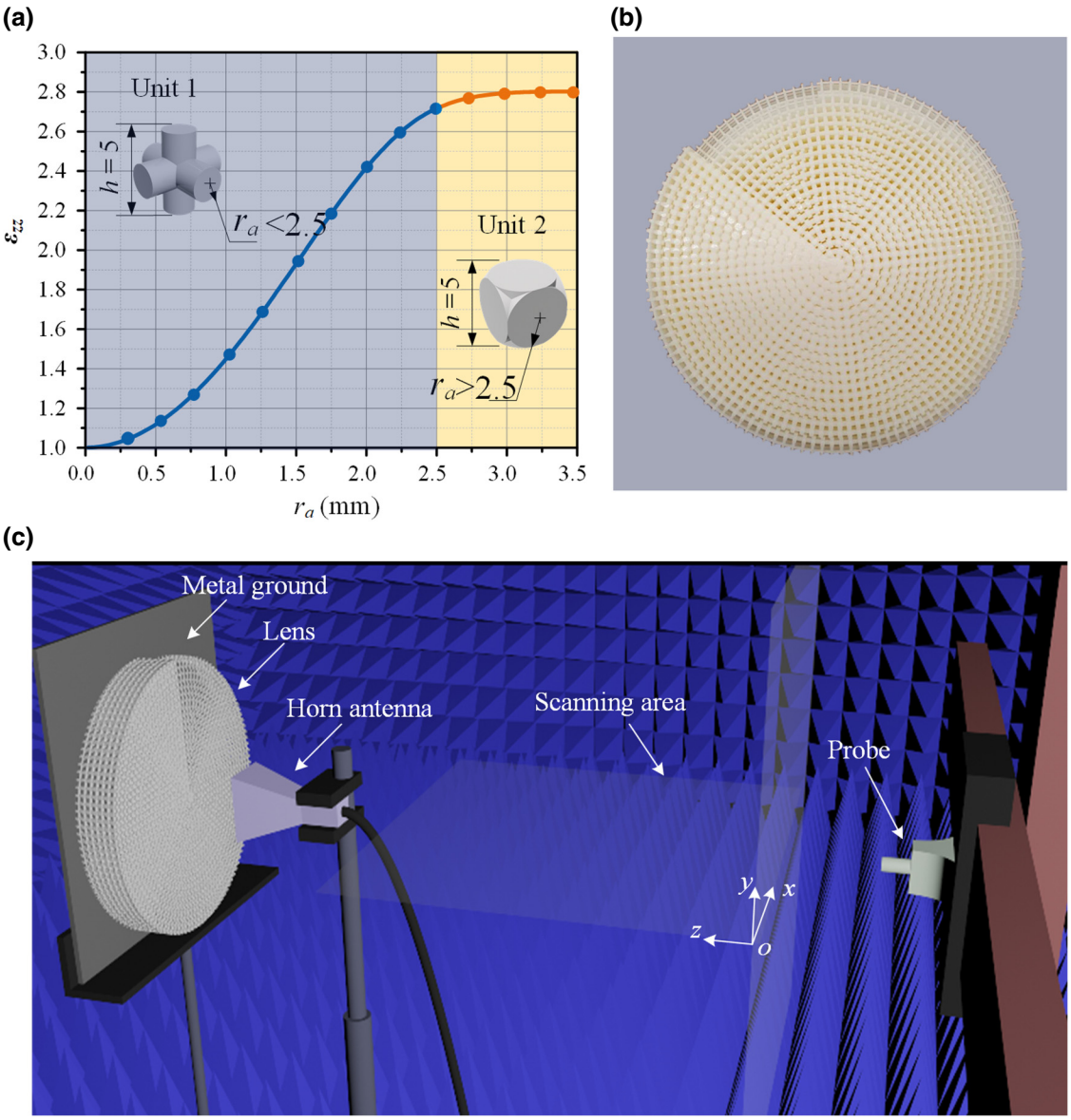

FIG. 3. (a) Effective permittivity of two types of unit cells used in the implementation of the device. A parametric analysis is performed to extract the effective permittivity from the homogenization procedure according to the radius r_a of each unit cell. (b) Photograph of the fabricated prototype created by polymer jetting 3D printing. (c) Experimental measurement setup of the proposed device in a microwave anechoic chamber.

recording the reflected field intensity and phase at every step, we acquire a full two-dimensional spatial-field mapping of the microwave electric field distribution in the x-o-y plane (located at a distance of z = 500 mm) over a total scanning surface of 400×400 mm^2. Secondly, far-field antenna radiation patterns are measured in an anechoic chamber, where a horn antenna is used as a receiver to measure the power emitted from the vortex-wave-generating system. Far-field measurements are performed for elevation angles ranging from -180° to 180°.

The measured phase distributions and intensity patterns at different frequencies are given in Fig. 4. In Fig. 4(a), when the incident and reflected waves pass through the dielectric device, the phase distribution shows a total 2π phase change in a helical configuration, which is characteristic of electromagnetic waves carrying an $l = +1$ OAM mode. The phase profiles measured from the vortex-beam generator are consistent with those achieved by simulations. As illustrated in Fig. 4(b), the intensity patterns measured with the OAM-generation device have a doughnut shape with a null at the center. As a comparison, the measured phase distributions and intensity patterns with the metallic plate alone at different frequencies are given in Supplemental Material [27]. Without the transformed material, concentric circular phase patterns and quasiregular intensity patterns of a plane wave are observed.

Additionally, the measured far-field patterns in the **E** and **H** planes are presented in Fig. 4(c). It can be clearly seen that the fabricated device produces "bunny ear"-shaped beams in the frequency band from 8 to 16 GHz. Furthermore, the OAM-mode purity calculated from the experimental data at different frequencies is presented in Fig. 4(d). It can be observed that generated OAM waves with the +1 mode still dominate, validating the

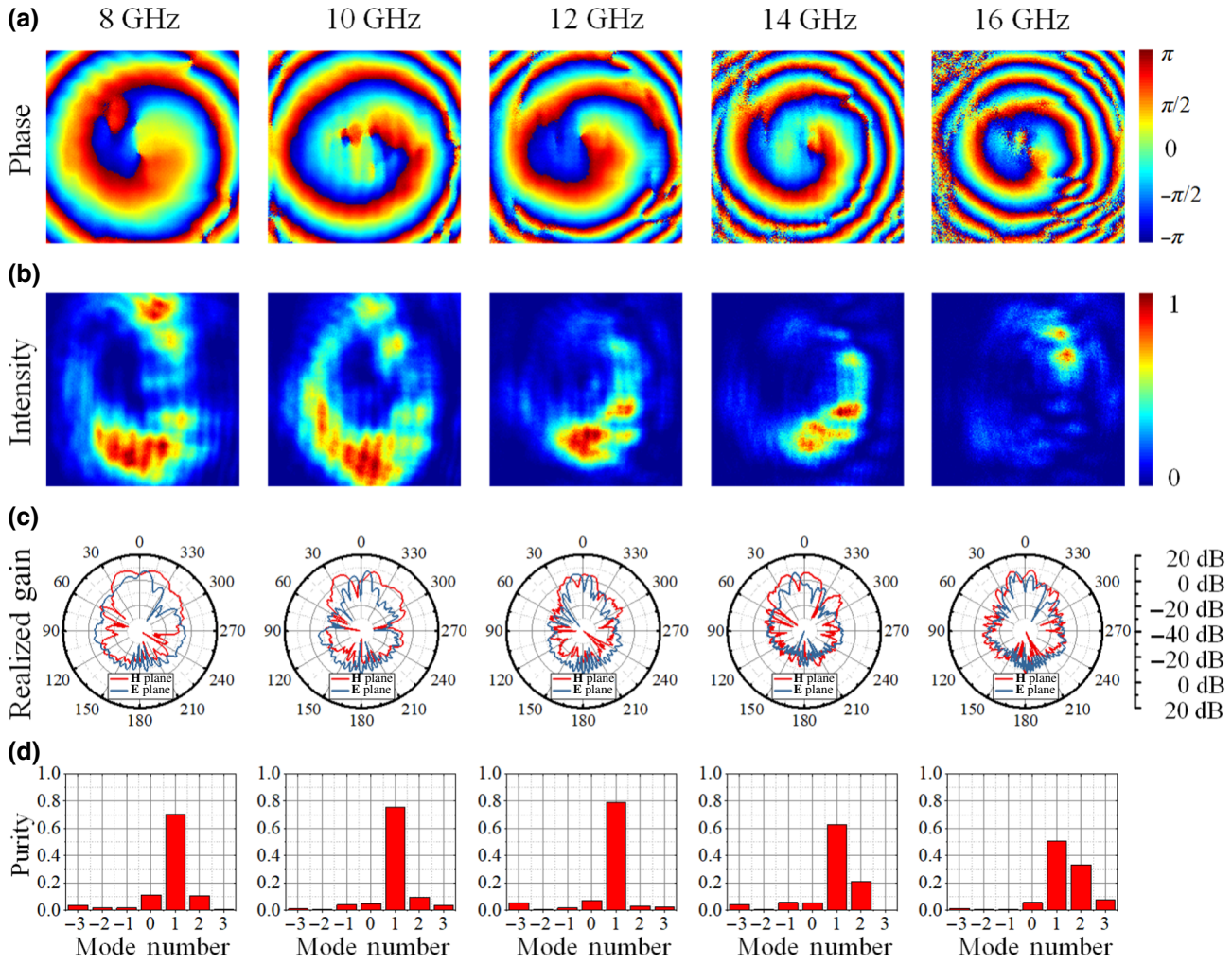

FIG. 4. Measured performances at 8, 10, 12, 14, and 16 GHz. (a) Phase distributions of the electromagnetic field in the x-o-y plane at a distance of 500 mm from the feed plane. The phase varies from $-\pi$ (blue) to π (red). (b) Intensity distributions of the electromagnetic field in the x-o-y plane at a distance of 500 mm from the feed plane. (c) Two-dimensional radiation patterns in the **H** and **E** planes. (d) Experimental mode spectra of the generated $l = +1$ OAM beam.

efficiency of the designed device. It is important to point out that the intensity distributions of the generated vortex waves are not fully homogeneous and the far-field radiated beams are slightly tilted. These two undesired phenomena can be attributed firstly to the quasi-isotropic material used to make the device and secondly to the superposition of other undesired generated modes. Indeed, the spatial-transformation process leads to an anisotropic transformed material. However, for the device implementation, anisotropy is ignored to keep only a distribution of ε_{zz} such that quasi-isotropic material can be used. In addition, in the generation of OAM waves carrying the $+1$ mode, some OAM waves with other modes are inevitably produced as observed from the mode spectra in Figs. 2(d) and 4(d). When waves carrying such undesired modes are superposed onto the desired $+1$-mode OAM wave, performance degradation as illustrated by the inhomogeneous field-intensity distributions and asymmetric radiation patterns is observed [30–32].

IV. CONCLUSIONS

In summary, on the basis of the concept of spatial transformation, we propose a universal method to transform an irregularly shaped virtual space into an all-dielectric microwave device with spatially varying permittivity that is capable of generating electromagnetic vortex waves carrying OAM in an effective manner. To validate the OAM characteristics, the device configuration is simulated for the generatation of vortex beams with a topological charge of $l = +1$. Furthermore, the reflection-type OAM generator is fabricated by additive manufacturing and experimentally characterized. Good qualitative agreement is obtained between full-wave simulations and measurements, indicating that a vortex spiral-shaped phase front and a hollow beam with high purity are successfully achieved. In addition, because of the nonresonant meta-atoms used in the implementation, the device is able to operate over a broad frequency range. Such spatial-transformation-based design methods offer an effective strategy for tailoring electromagnetic waves with nearly arbitrary desired properties. Moreover, because of the benefits of a wide operating bandwidth as well as the ease of fabrication and integration, the proposed approach is expected to have a profound impact on future OAM-based systems. Finally, some strategies can be considered to reduce the divergence of OAM beams, which can be a limitation for microwave-antenna applications. For instance, metasurfaces or even the transformation-optics concept can be used to design lenses for collimation of OAM beams [9,21,33].

ACKNOWLEDGMENTS

This work was supported by the National Natural Science Foundation of China (Grants No. 61601345 and No. 61601344), the Fundamental Research Funds for the Central Universities (rtant No. JB190118), and the Innovation Funding of Xidian University. This work was awarded Doctoral Students' Short-Term Study Abroad Scholarship Funding of Xidian University. The opinions in this work are solely those of the authors and do not necessarily reflect those of the U.S. Military Academy, the U.S. Army, or the U.S. Department of Defense.

[1] L. Allen, M. W. Beijersbergen, R. J. C. Spreeuw, and J. P. Woerdman, Orbital angular momentum of light and the transformation of Laguerre-Gaussian laser modes, Phys. Rev. A **45**, 8185 (1992).

[2] J. Tang, Y. Ming, Z. X. Chen, W. Hu, F. Xu, and Y. Q. Lu, Entanglement of photons with complex spatial structure in Hermite-Laguerre-Gaussian modes, Phys. Rev. A **94**, 012313 (2016).

[3] F. Tamburini, E. Mari, A. Sponselli, B. Thidé, A. Bianchini, and F. Romanato, Encoding many channels on the same frequency through radio vorticity: first experimental test, New. J. Phys. **14**, 033001 (2012).

[4] K. Liu, Y. Cheng, Z. Yang, H. Wang, Y. Qin, and X. Li, Orbital-angular-momentum-based electromagnetic vortex imaging, IEEE. Antennas. Wirel. Propag. Lett. **14**, 711 (2015).

[5] T. Yang, S. Li, O. Xu, W. Li, and Y. Wang, Three dimensional SAR imaging based on vortex electromagnetic waves, Remote Sensing Letters **9**, 343 (2018).

[6] M. Lin, Y. Gao, P. Liu, and J. Liu, Improved OAM-based radar targets detection using uniform concentric circular arrays, Int. J. Antennas. Propag. **2016**, 0 (2016).

[7] K. Liu, Y. Cheng, X. Li, and Y. Gao, Microwave-sensing technology using orbital angular momentum: Overview of its advantages, IEEE Vehicular Technology Magazine **14**, 112 (2019).

[8] F. E. Mahmouli, and S. D. Walker, 4-Gbps uncompressed video transmission over a 60-GHz orbital angular momentum wireless channel, IEEE Wireless. Commun. Lett. **2**, 223 (2013).

[9] Y. F. Meng, J. Yi, S. N. Burokur, L. Kang, H. L. Zhang, and D. H. Werner, Phase-modulation based transmitarray convergence lens for vortex wave carrying orbital angular momentum, Opt. Express **26**, 22019 (2018).

[10] S. Jiang, C. Chen, H. L. Zhang, and W. D. Chen, Achromatic electromagnetic metasurface for generating a vortex wave with orbital angular momentum (OAM), Opt. Express **26**, 6466 (2018).

[11] Z. H. Jiang, L. Kang, W. Hong, and D. H. Werner, Highly efficient broadband multiplexed millimeter-wave vortices from metasurface-enabled transmit-arrays of subwavelength thickness, Phys. Rev. A **9**, 064009 (2018).

[12] K. Zhang, Y. Y. Yuan, D. W. Zhang, X. M. Ding, B. Ratni, S. N. Burokur, M. J. Lu, K. Tang, and Q. Wu, Phase-engineered metalenses to generate converging and non-diffractive vortex beam carrying orbital angular momentum in microwave region, Opt. Express **26**, 1351 (2018).

[13] K. Zhang, Y. Yuan, X. Ding, B. Ratni, S. N. Burokur, and Q. Wu, High efficiency metalenses with switchable

functionalities in microwave region, ACS Applied Materials & Interfaces **11**, 28423 (2019).
[14] X. Hui, S. Zheng, Y. Hu, C. Xu, X. Jin, H. Chi, and X. Zhang, Ultralow reflectivity spiral phase plate for generation of millimeter-wave OAM beam, IEEE. Antennas. Wirel. Propag. Lett. **14**, 966 (2015).
[15] Y. Chen, S. Zheng, Y. Li, X. Hui, X. Jin, H. Chi, and X. Zhang, A flat-lensed spiral phase plate based on phase-shifting surface for generation of millimeter-wave OAM beam, IEEE. Antennas. Wirel. Propag. Lett. **15**, 1156 (2016).
[16] F. Tamburini, E. Mari, B. Thidé, C. Barbieri, and F. Romanato, Experimental verification of photon angular momentum and vorticity with radio techniques, Appl. Phys. Lett **99**, 204102 (2011).
[17] J. B. Pendry, D. Schurig, and D. R. Smith, Controlling electromagnetic fields, Science **312**, 1780 (2006).
[18] U. Leonhardt, Optical conformal mapping, Science **312**, 1777 (2006).
[19] A. Keivaan, M. H. Fakheri, A. Abdolali, and H. Oraizi, Design of coating materials for cloaking and directivity enhancement of cylindrical antennas using transformation optics, IEEE Antennas Wireless Propag. Lett **16**, 3122 (2017).
[20] J. Li, and J. B. Pendry, Hiding under the carpet: anew strategy for cloaking, Phys. Rev. Lett **101**, 203901 (2008).
[21] T. Liu, R. Feng, J. Yi, S. N. Burokur, C. Mao, H. Zhang, and D. H. Werner, All-dielectric transformation medium mimicking a broadband converging lens, Opt. Express **26**, 20331 (2018).
[22] J. Yi, S. D. Campbell, R. Feng, S. N. Burokur, and D. H. Werner, Realizable design of field taper via coordinate transformation, Opt. Express **26**, 505 (2018).
[23] N. Kundtz, and D. R. Smith, Extreme-angle broadband metamaterial lens, Nat. Mater **9**, 129 (2010).
[24] H. F. Ma, and T. J. Cui, Three-dimensional broadband and broad-angle transformation-optics lens, Nat. Commun. **1**, 124 (2010).
[25] C. Garcá-Meca, A. Martńez, and U. Leonhardt, Engineering antenna radiation patterns via quasi-conformal mappings, Opt. Express **19**, 23743 (2011).
[26] Q. Wu, Z. H. Jiang, O. Quevedo-Teruel, J. P. Turpin, W. Tang, Y. Hao, and D. H. Werner, Transformation optics inspired multibeam lens antennas for broadband directive radiation, IEEE Trans. Antennas Propag. **61**, 5910 (2013).
[27] See Supplemental Material at http://link.aps.org/supplemental/10.1103/PhysRevApplied.12.024064 for the detailed design of the OAM-vortex-beam-generation device and measured results with the metallic plate alone at different frequencies.
[28] B. Jack, M. Padgett, and S. Franke-Arnold, Angular diffraction, New J. Phys. **10**, 103013 (2008).
[29] Objet connex 3, https://www.stratasys.com/3d-printers/objet260-connex3.
[30] M. Barbuto, M.-A. Miri, A. Alu, F. Bilotti, and A. Toscano, Exploiting the topological robustness of composite vortices in radiation systems, Progress In Electromagnetics Research **162**, 39 (2018).
[31] E. Galvez, N. Smiley, and N. Fernandes, Composite optical vortices formed by collinear Laguerre-Gauss beams, in Nanomanipulation with Light II, Vol. 6131 (International Society for Optics and Photonics, 2006) p. 613105.
[32] M. Vasnetsov, I. Marienko, and M. Soskin, Self-reconstruction of an optical vortex, Journal of Experimental and Theoretical Physics Letters **71**, 130 (2000).
[33] Y. Jianjia, D. Li, R. Feng, B. Ratni, Z. Jiang, A. De Lustrac, D. H. Werner, and S. N. Burokur, Design and validation of a metasurface lens for converging vortex beams, Applied Physics Express **12**, 084501 (2019).